High Electrocatalytic Performance of Mn_3O_4/Mesoporous Carbon Composite for Oxygen Reduction in Alkaline Solutions

Yong-gang Wang, Liang Cheng, Feng Li, Huan-ming Xiong, and Yong-yao Xia*

Chemistry Department and Shanghai Key Laboratory of Molecular Catalysis and Innovative Materials, Fudan University, Shanghai 200433, People's Republic of China

Received November 11, 2006. Revised Manuscript Received February 1, 2007

The Mn_3O_4 nanoparticles (ca. 10 nm) were artificially loaded the on the outer surface of CMK-3, rather than forming within the pores of CMK-3, by utilizing the hydrophobic property of CMK-3 itself and its narrow pore size. The electrocatalytic performance for the oxygen reduction of the prepared Mn_3O_4/CMK-3 composite was extensively studied as an air diffusion electrode material in comparison with the composite catalysts based on the other carbons (carbon nanotubes, activated carbon, and graphite). The results of electrochemical tests indicate that the Mn_3O_4/CMK-3 composite can provide sufficient effective three-phase interface area due to the unique structures, which plays the important role in the complex three-phase interface electrocatalytic reaction. As a result, the composite electrode behaves with a much higher electrocatalytic performance for oxygen reduction than that of the composite catalysis based on the other carbons.

1. Introduction

In the past years, nanostructured carbon materials and carbon based composites have attracted great interest for the development of electronic systems,[1] hydrogen-storage systems,[2,3] electrode materials,[4−8] and catalytic reaction.[9−12] The self-ordered mesoporous carbon[13−16] with pore arrangements in hexagonal or cubic structures, having uniform mesopores and high surface area, has attracted great attention. Recently, self-ordered mesoporous carbon has been used as an ideal host for host−guest chemistry to synthesize high dispersion of nanoparticles,[17,18] in which the nanoparticles were constricted to grow within the mesopores of carbon to give them optimal dimensions.[18] Ryoo et al. reported that the platinum particle can be controlled to be less than 3 nm on the ordered nanoporous arrays of carbon, and the high dispersions of platinum nanoparticles have high electrocatalytic performance of oxygen reduction in $HClO_4$ solution saturated with O_2.[17] The high electrocatalytic performance reported by Ryoo is ascribed to that the high dispersive platinum nanoparticles increase the effective two-phase interface area (catalyst particles/$HClO_4$ solution saturated with O_2), thus resulting in the high utilization of platinum particles. Following their work, many research groups also applied the high dispersive platinum nanoparticles in the electrocatalytic reaction of direct methanol fuel cell (DMFC)[19−22] (reaction occurring at the interface of methanol solution/platinum nanoparticle).

In a real fuel cell or air−metal battery, the electrocatalytic oxygen reduction reaction in the gas diffusion electrode is a typical "three-phase interface electrocatalytic reaction". The gas must continuously diffuse into the electrode and take part in the electrocatalytic reaction. Accordingly, both the effective gas diffusion path and sufficient effective three-phase interface area (gas−catalyst−electrolyte solution) are very necessary for "three-phase interface electrocatalytic

* Corresponding author. Fax: (+86)-21-55664177. E-mail: yyxia@fudan.edu.cn.

(1) (a) Fan, S.; Wang, J. A.; Yuan, R.; Ma, Y.; Meng, Q.; Erdos, M. R.; Pestell, R. G.; Yuan, F.; Auborn, K. J.; Goldberg, I. D.; Rosen, E. M. *Science* **1999**, *283*, 512. (b) Rueckes, T.; Kim, K.; Joselevich, E.; Tseng, G. Y.; Cheung, C. Li.; Lieber, C. M. *Science* **2000**, *289*, 94.
(2) (a) Dillion, A. C.; Jones, K. M.; Bekkedahl, T. A.; Kiang, C. H.; Bethune, D. S.; Heben, M. J. *Nature* **1997**, *386*, 337. (b) Lin, J. *Science* **2000**, *287*, 1929.
(3) Fang, B. Z.; Zhou, H. S.; Honma, I. *J. Phys. Chem. B* **2006**, *110*, 4875.
(4) (a) Zhou, H. S.; Zhu, S. M.; Hibino, M.; Honma, I.; Ichihara, M. *Adv. Mater.* **2003**, *15*, 2107. (b) Furukawa, H.; Hibino, M.; Zhou, H. S.; Honma, I. *Chem. Lett.* **2003**, *32*, 132.
(5) Fan, J.; Wang, T.; Yu, C. X.; Tu, B.; Jiang, Z. J.; Zhao, D. Y. *Adv. Mater.* **2004**, *16*, 1432.
(6) Dong, X. P.; Shen, W. S.; Gu, J. L.; Xiong, L. M.; Zhu, Y. F.; Zhu, Y. F.; Li, H.; Shi, J. L. *J. Phys. Chem. B* **2006**, *110*, 6015.
(7) (a) Wang, Y. G.; Li, H. Q.; Xia, Y. Y. *Adv. Mater.* **2006**, *18*, 2619. (b) Wang, Y. G.; Yu, L.; Xia, Y. Y. *J. Electrochem. Soc.* **2006**, *153*, A743.
(8) Lee, C. Y.; Tsai, H. M.; Chuang, H. J.; Li, S. Y.; Lin, P.; Tseng, T. Y. *J. Electrochem. Soc.* **2005**, *152*, A716.
(9) Kim, Y. T.; Ohshima, K.; Higashimine, K.; Uruga, T.; Takata, M.; Suematsu, H.; Mitani, T. *Angew. Chem., Int. Ed.* **2006**, *45*, 407.
(10) Villani, K.; Kirschhock, C. E. A.; Liang, D.; Tendeloo, G. V.; Martens, J. A. *Angew. Chem., Int. Ed.* **2006**, *45*, 3106.
(11) Yang, H.; Vante, N. A.; Lamy, C.; Akins, D. L. *J. Electrochem. Soc.* **2005**, *152*, A704.
(12) Choi, W. C.; Woo, S. I.; Jeon, M. K.; Sohn, J. M.; Kim, M. R.; Jeon, H. J. *Adv. Mater.* **2005**, *17*, 446.
(13) Kyotani, T.; Tsai, L.; Tomita, A. *Chem. Commun.* **1997**, 701.
(14) Kruk, M.; Jaroniec, M.; Ryoo, R.; Joo, S. H. *J. Phys. Chem. B* **2000**, *104*, 7960.
(15) Jun, S.; Hoo, S. H.; Ryoo, R.; Kruk, M.; Jaroniec, M.; Liu, Z.; Ohsuna, T.; Terasaki, O. *J. Am. Chem. Soc.* **2000**, *122*, 10712.
(16) Han, S.; Hyeon, T. *Chem. Commmun.* **1999**, 1995.
(17) Joo, S. H.; Choi, S. J.; Oh, I.; Kwak, J.; Liu, Z.; Teraski, O.; Ryoo, R. *Nature* **2001**, *412*, 169.
(18) Zhu, S. M.; Zhou, H. S.; Hibino, M.; Honma, I.; Ichilara, M. *Adv. Funct. Mater.* **2005**, *15*, 381.
(19) Chai, G. S.; Yoon, S. B.; Yu, J. S.; Choi, J. H.; Sung, Y. E. *J. Phys. Chem. B* **2004**, *108*, 7074.
(20) (a) Raghuveer, V.; Manthiram, A. *J. Electrochem. Soc.* **2004**, *7*, A336. (b) Raghuveer, V.; Manthiram, A. *J. Electrochem. Soc.* **2005**, *152*, A1504.
(21) Su, F. B.; Zeng, J. H.; Bao, X. Y.; Yu, Y. S.; Lee, J. Y.; Zhao, X. S. *Chem. Mater.* **2005**, *17*, 3960.
(22) Blanco, J.; Petre, A. L.; Yates, M.; Martin, M. P.; Suarez, S.; Martin, J. A. *Adv. Mater.* **2006**, *18*, 1162.

10.1021/cm062685t CCC: $37.00
Published on Web 03/17/2007

reaction". The rate of the gas diffusion process can affect the rate of the electrocatalytic process greatly. However, very few works have been devoted to design an advanced functional material to improve the electrocatalytic performance of the oxygen reduction. However, this work is very necessary, because improving the electrochemical performance of fuel cells or air−metal batteries has attracted global attention.[23] Therefore, the preparation of advanced carbon based catalyst for a complex "three-phase interface electrocatalytic reaction" would appear to be of great interest.

On the other hand, manganese oxides MnO_x (such as MnO_2, Mn_2O_3, Mn_3O_4, and Mn_5O_8) have been demonstrated to be one of the most promising catalysts for oxygen reduction because of their low cost and relative high electrocatalytic activity. In recent years, many efforts have been made to evaluate and optimize the electrocatalytic performance of carbon supported MnO_x catalysts. For example, Zhang et al. reported that gas diffusion electrode based on MnO_x/carbon nanotubes composites exhibit higher electrocatalytic performance of oxygen reduction than that of the other carbon based catalyst (MnO_x).[24] The nanowire's network of carbon nanotubes can form random interconnected pore structure, which can increase the effective three-phase interface area. However, the catalyst layer structure for the three-phase interface electrocatalytic reaction is not optimized enough because the gas cannot go through the carbon wall and contact the catalyst particles directly; in addition, the hollow nature of carbon nanotubes could be used for gas storage.

Herein, we for the first time report a Mn_3O_4/carbon composite catalyst based on self-ordered mesoporous carbon, in which Mn_3O_4 nanoparticles (ca. 10 nm) were artificially loaded on the outer surface of ordered mesoprous carbon (CMK-3) by utilizing the hydrophobic property of CMK-3 itself and its narrow pore size, rather than the nanoparticles (Pt, less than 4 nm) formed inside the carbon mesopores.[17,18] The electrocatalytic performance for the oxygen reduction of the prepared Mn_3O_4/CMK-3 composite was extensively studied as an air diffusion electrode material in comparison with the composite catalysts based on the other carbons (carbon nanotubes, activate carbon, and graphite).

2. Experiment

2.1. Preparation and Characterization. Mesoporous silica SBA-15 is used as the template and was prepared according to the reported procedure.[25] The mesoporous carbon CMK-3 was prepared by the method reported by Jun et al.[15] The preparation process for CMK-3 was described as follows: 1 g of SBA-15 was added to a solution obtained by dissolving 1.25 g of sucrose and 0.14 g of H_2SO_4 in 5 g of H_2O. After stirred under a vacuum of 0.1 MPa for 20 min the mixture was placed in a drying oven for 6 h at 100 °C and another 6 h at 160 °C. The carbonization was completed by pyrolysis at 900 °C under N_2 flow. Finally the carbon−silica composite obtained after pyrolysis was washed with 5 wt % hydrofluoric acid at room temperature to remove the silica template.

The preparation process of the Mn_3O_4/CMK-3 composite can be described as follows: 0.1 g of CMK-3 was added in 100 mL of 20 wt % ethanol ($H_2O-CH_3CH_2OH$ mixed solution) that containing $Mn(NO_3)_2$, and then the solvent was vaporized at 80 °C for 1 h under stirring. Finally, the Mn_3O_4/CMK-3 composite was obtained by heat-treatment of the mixture of $Mn(NO_3)_2$ and CMK-3 at 350 °C for 2 h with a heating rate of 5 °C/min under pure N_2 flow. For the comparison, the Mn_3O_4/multiwalled carbon nanotubes (MWNTs), Mn_3O_4/activated carbon, and Mn_3O_4/graphite composite were also prepared by the same procedure as described above. For the Mn_3O_4/MWNTscomposite, MWNTs were first sonicated in 30% HNO_3 solution for 30 min, then filtered and washed with distilled water, and finally dried at 100 °C for 12 h. For all composites, the mass load of the Mn_3O_4 in the composite was controlled at 25 wt %.

The as-prepared samples were characterized by X-ray diffraction (XRD, Bucker D8), scanning electronic microscopy (SEM, Philip XL30), transmission electron microscopy (TEM, Jeol JEM-2010), and BET surface area measurement (Micromeritics Tristar).

The Mn_3O_4/carbon composites were used as an air diffusion electrode material to study the electrocatalytic performance for the oxygen reduction. The gas diffusion electrode consists of a catalyst layer, a gas diffusion layer, and a current accumulating matrix. The catalyst layer was prepared as follows: The mixture of Mn_3O_4/carbon materials catalyst (80 wt %), conductive graphite (5 wt %), and polytetrafluoroethylene (PTFE) emulsion (15%) was well mixed, and then it was roller-pressed into an approximately 0.1 mm thick sheet. The gas diffusion layer was prepared by mixing acetylene black (60 wt %) and PTFE emulsion (40 wt %) with isopropanol into paste and then rolling the paste into 0.5 mm thick film. The gas diffusion layer was further immersed and refluxed in acetone for 24 h to enhance hydrophobicity before using. The three layer gas electrode was finished by pressing the catalyst layer and gas diffusion layer onto a nickel mesh at 100 kg cm^{-2} into a 0.3 mm thick sheet. The area of the gas electrode was 0.5 cm^2, and the mass load of Mn_3O_4/carbon composite catalyst layer was 10 mg/cm^2.

2.2. Electrochemical Measurements. The cyclic voltammetry (CV) tests at a scan rate of 10 mV/s within the potential window $0 \sim 0.6$ V (vs SCE) and chronoamperometry technique at a applied potential of −0.3 V (vs SCE) were employed to characterize the polarization characterization of the gas diffusion electrodes using a three-electrode cell, in which the platinum and saturated calomel electrode (SCE, 0.242 V vs NHE) were used as the counter and reference electrodes. A gel alkaline electrolyte solution containing 6 M KOH was used. The preparation of gel alkaline electrolyte and the cell configuration was similar to that reported by Zhang et al.[24] The electrochemical experiments were performed using a Solartron Instrument model 1287 electrochemical interface controlled by a computer.

3. Results and Discussion

3.1. Preparation and Characterization. Figure 1 gives the wide-angle XRD patterns of MnO_x/CMK-3 composite and CMK-3. As shown in Figure 1A, the XRD pattern of MnO_x/CMK-3 composite shows the diffraction peaks at 29°, 31°, 32.4°, 36.1°, 38.1°, 44.4°, 50.8°, 58.5°, 59.9°, and 64.6°, which can be ascribed to the characteristic peaks of the Mn_3O_4. The average Mn_3O_4 particle sizes in the Mn_3O_4/CMK-3 composite were estimated to be 8.7 nm on the basis of the Mn_3O_4 (211) peak by Scherrer's equation. Figure 1B shows the XRD patterns of CMK-3, in which two character

(23) (a) Steele, B. C. H.; Heinzel, A. *Nature* **2001**, *414*, 345. (b) Service, R. F. *Science* **2002**, *296*, 1222. (c) Schlapbach, L.; Züttel, A. *Nature* **2001**, *414*, 353. (d) Matsuoka, K.; Iriyama, Y.; Abe, T.; Matsuoka, M.; Ogumi, Z. *J. Power Sources* **2005**, *150*, 27.
(24) Zhang, G. Q.; Zhang, X. G.; Wang, Y. G. *Carbon* **2004**, *42*, 3097.
(25) Zhao, D. Y.; Feng, J.; Huo, Q.; Melosh, N.; Fredirckson, G. H.; Chemlka, B. F.; Stucky, G. D. *Science* **1998**, *279*, 548.

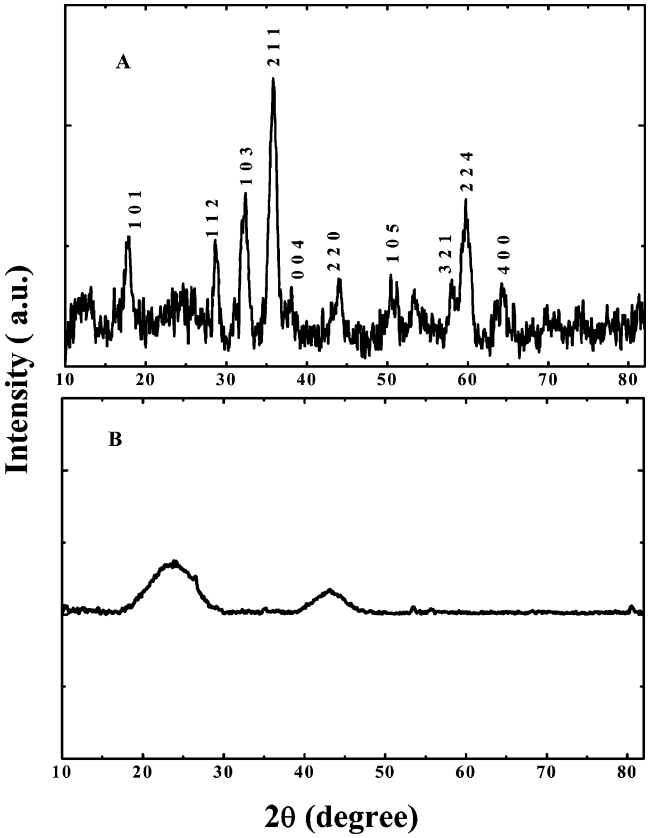

Figure 1. XRD patterns of Mn_3O_4/CMK-3 composite (A) and CMK-3 (B).

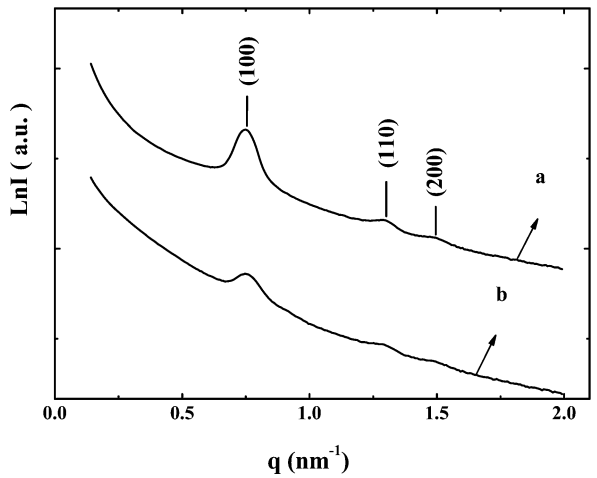

Figure 2. SAXS patterns of CMK-3 (a) and Mn_3O_4/CMK-3 composite (b).

diffraction peaks located at 24° and 43° were observed. The small-angle X-ray scattering (SAXS) of CMK-3 and Mn_3O_4/CMK-3 composite are shown in Figure 2. Both curves of Figure 2 (curve a and curve b) show the presence of the (100), (110), and (200) diffractions, indicating that loaded Mn_3O_4 does not change highly ordered two-dimensional hexagonal microstructure.

The morphologies and microstructures of carbon support materials (CKM-3) were examined by SEM and TEM. Figure 3 shows typical SEM and TEM images of CMK-3. SEM observation shown in Figure 3A shows that the prepared CMK-3 is column grains with a diameter of around 0.5 um and a length of about 1 μm. The TEM images of the

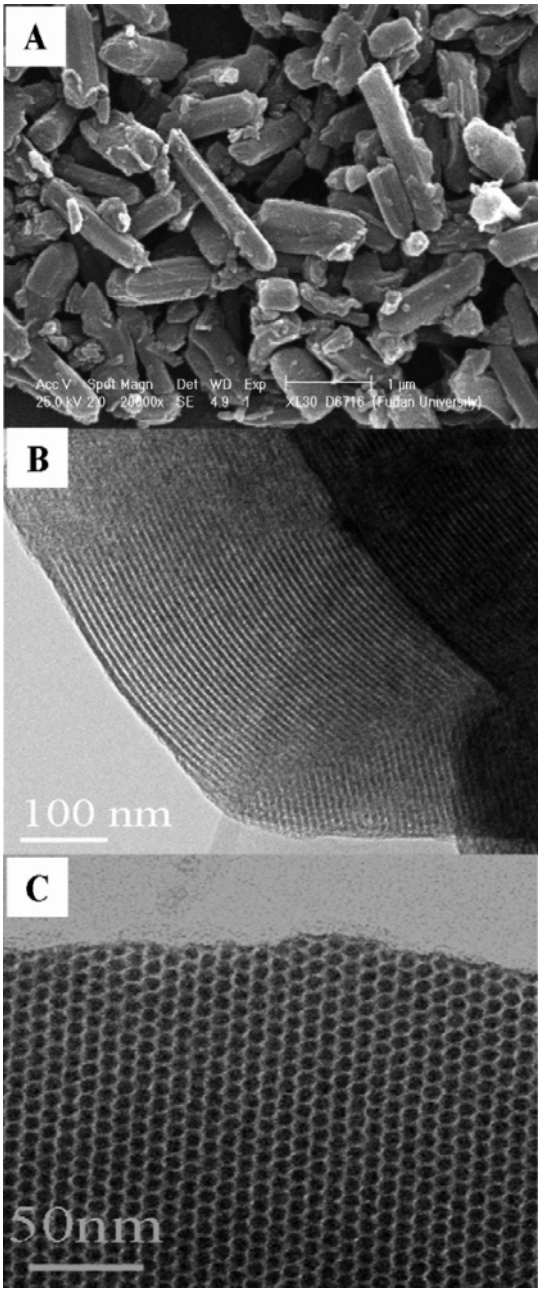

Figure 3. SEM images of Mn_3O_4 (A). TEM images of CMK-3 seen from [100] and [001] directions (B and C).

mesoporous carbon shown in Figure 3B,C display highly ordered carbon nanowires viewed from the [110] and [100] directions, and these wires are in the same perfect hexagonally mesostructured arrays as the channels of their mother mold SBA-15. The diameter of these nanowires is about 7 nm, the centers of adjacent wires are 10 nm apart, and thereby the distance between two nanowires is about 3 nm. Moreover, the interconnected space between the carbon nanowires was also observed clearly from [110] and [100] directions (see Figure 3B,C). Figure 4 gives the TEM images of the Mn_3O_4/CMK-3 composite. As shown in Figure 4A, a lot of Mn_3O_4 particles were loaded on the external surface of the mesoporous carbon. The higher-magnification TEM images of the Mn_3O_4/CMK-3 composite shown in Figure 4B,C reveal that the typical size of Mn_3O_4 particles on the surface of CMK-3 is about 10 $\pm$ 2 nm, which is in good

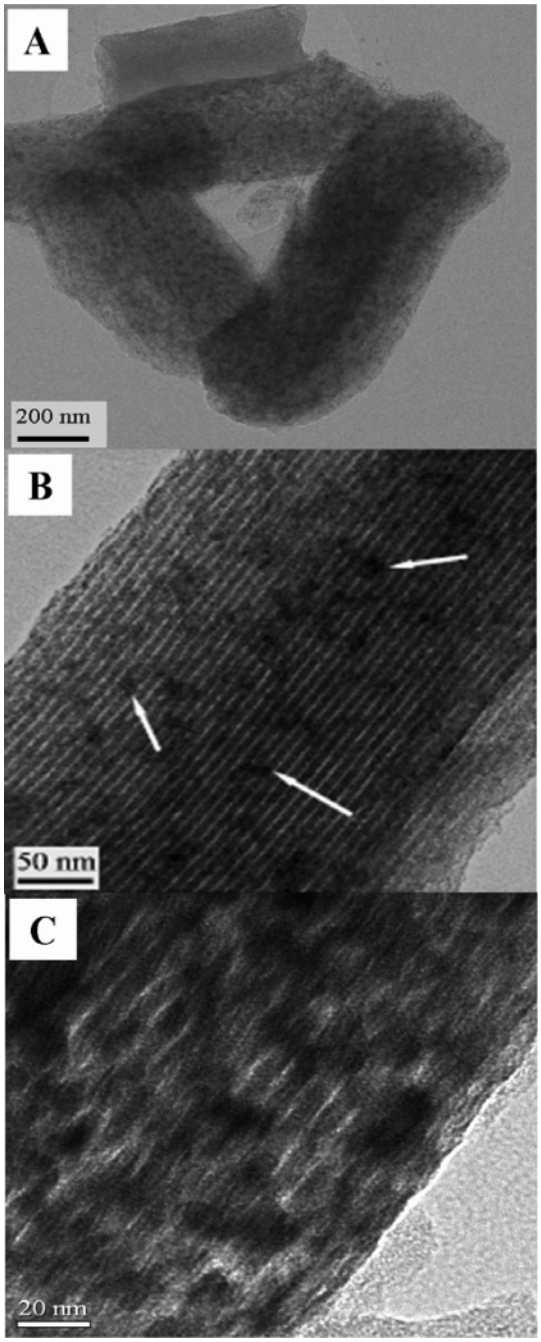

Figure 4. TEM images of Mn_3O_4/CMK-3 composite at different magnifications.

agreement with the calculated value from XRD patterns in Figure 2. From these findings, we speculate that these Mn_3O_4 particles are mainly loaded on the outer surface rather than inside the pores because the particle size of the Mn_3O_4 is much larger that surface-to-surface distance of the carbon nanowires (about 3 nm). This result was further confirmed by the result of N_2 adsorption−desorption isotherms and the pore volume and pore size distribution curves of CMK-3 in comparison with Mn_3O_4/CMK-3 composite.

Figure 5 shows the N_2 adsorption−desorption isotherms and the Barrett−Joyner−Halanda (BJH) calculations for pore volume and pore size distribution curves of CMK-3 as well as Mn_3O_4/CMK-3 composite. Both CMK-3 and Mn_3O_4/CMK-3 composite present a clear hysteresis loop within the relative pressure range of ~0.4−0.8, indicating its mesoporous structure (see Figure 5A). As shown in Figure 5B, the pore size distributions of CMK-3 and Mn_3O_4/CMK-3 composite all center at about 3.9 nm. This result can prove that Mn_3O_4 particles are mainly loaded on the outer surface of CMK-3. In other words, if a lot of Mn_3O_4 particles were formed within the porous structure of CMK-3, the pore size distributions of Mn_3O_4/CMK-3 composite would less than 3.9 nm greatly. The BET surface areas and total pore volume of both samples determined from the adsorption data are summarized in Table 1.

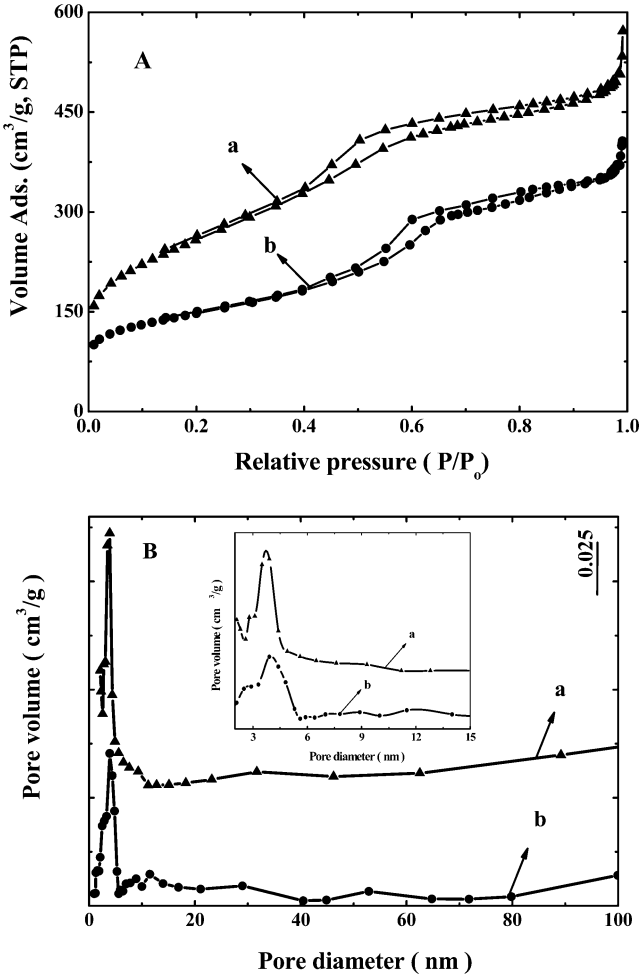

Figure 5. Adsorption−desorption isotherms (A) and the pore-size distributions (B) of CMK-3 and Mn_3O_4/CMK-3 composite. (a) CMK-3 and (b) Mn_3O_4/CMK-3 composite.

Table 1. BET Surface Area and Total Pore Volume of CMK-3 and Mn_3O_4/CMK-3 Composite

parameter	CMK-3	Mn_3O_4/CMK-3
S_{BET} (m^2/g)	920	521
total pore volume (cm^3/g)	0.88	0.63

As shown Table 1, the total pore volumes of CMK-3 and Mn_3O_4/CMK-3 composite are 0.88 cm^3/g and 0.63 cm^3/g, respectively, where the total pore volumes of Mn_3O_4/ CMK-3 composite were calculated by the following equation:

$$V_m = \frac{V}{m_{\text{CMK-3}} + m_{\text{Mn}_3\text{O}_4}} \quad (1)$$

where V is the pore volume (cm^3), $m_{\text{CMK-3}}$ is the mass of supporter (CMK-3), and $m_{\text{Mn}_3\text{O}_4}$ is the mass load of the Mn_3O_4

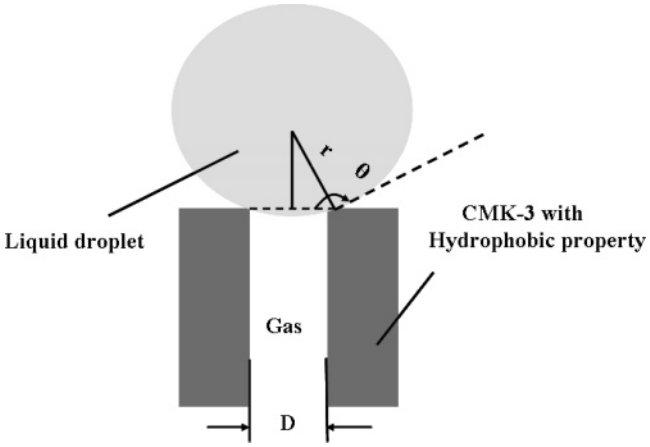

Figure 6. Simple model with a liquid droplet on the surface of hydrophobic CMK-3.

particles on the surface of CMK-3. For this instance, the weight ratio of Mn_3O_4 to CMK-3 is 1/3, and we assume that the Mn_3O_4 particle itself does not contribute much by way of pore volume; the total pore volume of CMK-3 within the Mn_3O_4/CMK-3 composite is 0.83 cm^3/g based on the sole weight of CMK-3. This result can also suggest that the Mn_3O_4 particles are mainly loaded on the outer surface of CMK-3.

It is most interesting to understand why the Mn_3O_4 particles are mainly loaded on the outer surface of CMK-3 rather than inside pores of CMK-3. To illustrate this phenomenon, a simple model with a liquid on the surface of hydrophobic CMK-3 can be built as Figure 6. As shown in Figure 6, the liquid dropt can be formed at the interface (liquid solution/outer surface of CMK-3), which is due to the hydrophobic property of CMK-3 itself. The relation between the pore size and the size of liquid droplet can be summarized by eq 2:

$$\sin\theta = \frac{D}{2r} \tag{2}$$

where the θ is the equilibrium contact angle on the surface of CMK-3. (θ is within the range 90−180°. The value of θ increases with the decrease of hydrophobic property.) r is the radius of the liquid droplet. D is the pore size of CMK-3. According to eq 2, the penetration ability of the liquid phase is critically dependent on the hydrophobic property and pore size of the microstructure. It means that the liquid droplet can be introduced by adjusting hydrophobic property and/or pore size. This process has been proved by Zhou et al.[18] In their study, the CMK-3 was first made to become hydrophilic by surface modification. Then, $KMnO_4$ solution was introduced to the pores of CMK-3. At last, MnO_2 nanoparticles with typical size ~2−3 nm were formed within the pores of CMK-3. On the other hand, Ryoo et al. used acetone as a solvent to dipresse H_2PtCl_6, rather than water solution. The hydrophobic organic solvent can penetrate the pores of carbon supporter easily. For this reason, platinum particle with typical size less than 3 nm was deposited inside the ordered nanopores of carbon supporter.[17] In the present work, the preparation process mainly involves: (1) Immerging CMK-3 (without hydrophilic treatment) in 20% ethanol

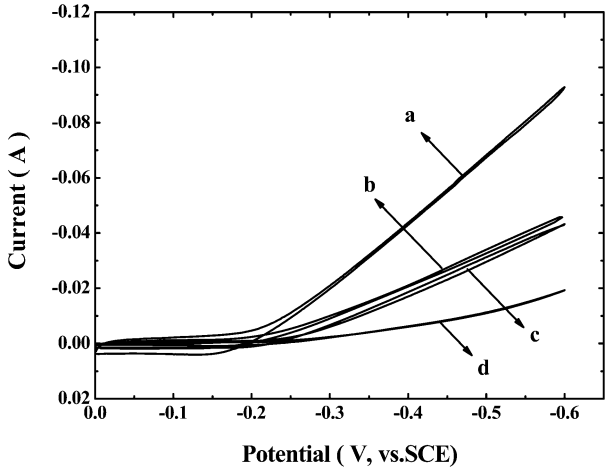

Figure 7. CV curves (at a scan rate of 10 mV/s) of gas diffusion electrodes based on (a) Mn_3O_4/CMK-3, (b) Mn_3O_4/MWNTs, (c) Mn_3O_4/AC, and (d) Mn_3O_4/graphite.

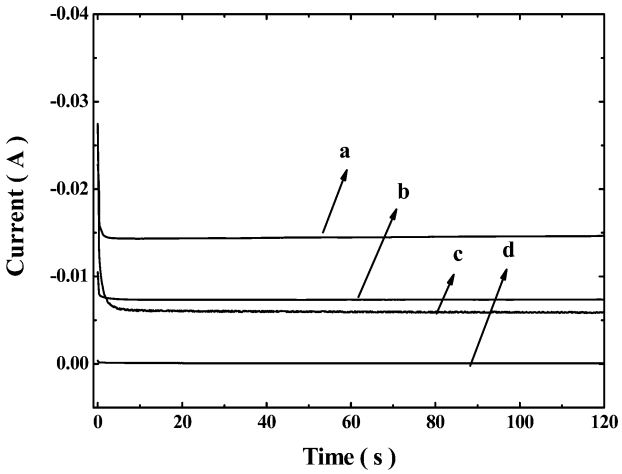

Figure 8. Chronoamperometry tests of air diffusion electrode based on (a) Mn_3O_4/CMK-3, (b) Mn_3O_4/MWNTs, (c) Mn_3O_4/AC, and (d) Mn_3O_4/graphite.

solution ($H_2O-CH_3CH_2OH$ mixed solution) containing certain $Mn(NO_3)_2$ under stirring condition. In this step, the $Mn(NO_3)_2$ solution can wet the external surface of CMK-3. However, it cannot flood these carbon pores within CMK-3, because the hydrophobic property of CMK-3 itself, the narrow pore size of CMK-3, and adsorbed air within these pores can prevent the penetration of $Mn(NO_3)_2$ solution. It was reported that water could not be introduced into the film when the hydrophobic microstructure scale was less than a certain size.[26] (2) Then the solvent was removed at 80 °C for under stirring; in this step, the "$Mn(NO_3)_2$ particles" were loaded on the outer surface of CMK-3. (c) Finally, $Mn(NO_3)_2$ particles turn to Mn_3O_4 on the outer surface of CMK-3 by heat treatment at 350 °C for 2 h under pure N_2 flow. As mentioned above, the key step of the preparation process is step 1. In this step, the $Mn(NO_3)$ solution cannot intrude the pores of CKM-3, which is due to the hydrophobic property of CMK-3 itself and the narrow pore size.[18]

3.2. Electrochemical Tests. The electrocatalytic performance of the air diffusion electrode based on Mn_3O_4/CMK-3

(26) (a) Li, S. H.; Li, H. J.; Wang, X. B.; Song, Y. L.; Liu, Y. Q.; Jiang, L.; Zhu, D. B. *J. Phys. Chem. B* **2002**, *106*, 9274. (b) McCarthy, T. J.; Oner, D. *Langmuir* **2000**, *16*, 7777.

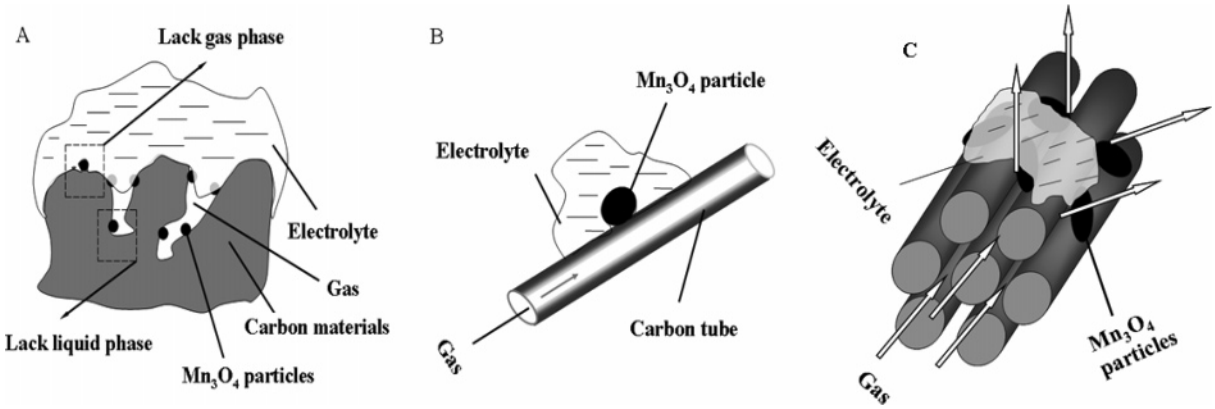

Figure 9. Schematic representation of the structure of different carbon based catalysts. (A) Mn_3O_4/AC, (B) Mn_3O_4/MWNTs, and (C) Mn_3O_4/CMK-3.

catalyst for the oxygen reduction was characterized by cyclic voltammograms (CV) in gel alkaline solution. Figure 7 compares the CV curves of the air diffusion electrodes based on Mn_3O_4/CMK-3 composite catalyst and Mn_3O_4 catalyst supported by other carbon materials. As shown in Figure 7, the cathodic current of all air electrodes starts to emerge at about −0.2 V (vs SCE) and increases rapidly as the potential becomes more negative, which is due to the reduction of oxygen. The results of CV clearly reveal that the electrocatalytic performance of air electrode based on Mn_3O_4/CMK-3 composite catalyst is higher than that of air electrode based on other carbon based Mn_3O_4 catalysts. It also should be noted that in none of the cases did the polarization curves show sharp rise of the electrode overpotential, indicating that the diffusion limitations within these electrodes are not apparent. To further compare the electrocatalytic performance of these carbon based composite catalysts, the chronoamperometry technique was also employed to compare the electrode polarization. As shown in Figure 8, after the potential jump from −0.15 V (vs SCE) to −0.3 V (vs SCE) is applied, the cathodic currents of all air diffusion electrodes increases sharply within a very short time (about 0.1 s). Then, the current density reduced quickly and achieved a constant value. However, the current of air diffusion electrode based on Mn_3O_4/CMK-3 is higher than that of air diffusion electrodes based on other composite catalysts clearly. This result can also suggest that the electrocatalytic performance of Mn_3O_4/CMK-3 composite is higher than that of other carbon based Mn_3O_4 catalysts.

The results of Figures 7 and 8 have proved that the Mn_3O_4/CMK-3 composite has higher electrocatalytic performance. At same time, the obvious diffusion limitations were not observed within all these electrodes. Thus we conclude that the higher electrocatalytic performance of Mn_3O_4/CMK-3 composite mainly arises from the extension of the reaction zone. In other words, the unique structure of Mn_3O_4/CMK-3 composite can provide more effective three-phase interface areas which increase the utilization of Mn_3O_4 particles. To illustrate this phenomenon, several simple models are built for different carbon based catalysts, and the relation between their structure and their electrocatalytic performance is also discussed simply. As shown in Figure 9A, the porous structure of activated carbon (AC) is not uniform (its pores size ranges from 1 nm to 100 nm). When electrolyte penetrates in these pores, some catalyst particles are flooded by electrolyte and some catalyst particles cannot contact the electrolyte totally (labeled by arrowhead, see Figure 9A). Thus the effective three-phase interface areas (or reaction zone) within the Mn_3O_4/AC composite are not sufficient. The nanowire's network of carbon nanotubes can form random interconnected pore structure (its pore size distribution is located at about 50−60 nm), which can increase the effective reaction zone.[24] However, as shown in Figure 9B, in this kind of carbon based catalyst the drawback still exists of direct contact of the gas phase. Although the hollow nature of the carbon nanotubes could be used for gas storage and diffusion, the gas cannot go through the carbon wall and contact the catalyst particles directly (see Figure 9B). As for Mn_3O_4/CMK-3 shown in Figure 9C, the situation is totally different because the Mn_3O_4 nanoparticles were artificially loaded the on the outer surface of CMK-3 rather than inside the carbon pores of CMK-3. The hydrophobic property of CMK-3 itself, its narrow pore size (3−4 nm), and adsorbed gas within pores can reduce the penetration of electrolyte solution. Thus, these ordered and interconnected pores can be used as the diffusion channels. The Mn_3O_4 nanoparticles loaded on the outer surface of CMK-3 can contact the electrolyte solution on the external surface of CMK-3 adequately (see Figure 9C). At same time, these Mn_3O_4 nanoparticles can also touch the gas stored in the bulk of CMK-3 easily (see Figure 9C), because all of the pores within CMK-3 are interconnected. For these reasons, sufficient effective three-phase interfacial area is available for electrocatalytic reaction. In brief, the unique structure of this composite can provide more effective three-phase interface area, thus resulting in its higher electrocatalytic performance. In summary, specific surface area and porous structure of carbon materials are very important for the electrocatalytic performance of carbon based catalysts. For example, the specific surface area of the Mn_3O_4/AC composite is about 2000 m^2/g, which is much higher than that of Mn_3O_4/graphite composite (7 m^2/g). Thus, the former has higher performance. On the other hand, the porous structure can also affect the electrocatalytic performance greatly. For instance, the specific surface area of Mn_3O_4/MWNTs is just 80 m^2/g, which is much smaller than that of Mn_3O_4/AC composite. However, its electrocatalytic performance is close to that of Mn_3O_4/AC composite. The reason is that nanowire's network of carbon nanotubes can form random interconnected porous structure, which increases the effective

three-phase interface area. The Mn_3O_4/CMK-3 composite has not only ordered interconnected porous structure but also high specific surface area (520 m^2/g), thus resulting in its higher electrocatalytic performance. It also should be noted that the Mn_3O_4 particles loaded on CMK-3 and Mn_3O_4 particles loaded on MWNTs are the same size (about 10 ± 2 nm). (The TEM image and XRD pattern of Mn_3O_4/MWNTs are not shown in this paper.) This result also suggests electrocatalytic performance at the three-phase interface is mainly affected by structure of catalysts, rather than the size of catalysts.

4. Conclusion

In summary, Mn_3O_4 nanoparticles (ca. 10 nm) were artificially loaded on the outer surface of CMK-3, rather than inside these mesopores. As an air diffusion electrode material for the oxygen reduction, the ordered interconnected pores within the bulk of CMK-3 can provide effective gas diffusion channels. Consequently, the Mn_3O_4 nanoparticles loaded on the surface of CMK-3 can get sufficient three-phase interface area, which is very important for "complex three-phase interface electrocatalytic reaction". The result of electrochemical tests indicates that the electrocatalytic performance of the Mn_3O_4/CMK-3 composite for oxygen reduction is much higher than that of other carbon based composite catalysts (Mn_3O_4/MWNTs composite, Mn_3O_4/AC composite, and Mn_3O_4/graphite composite). The higher electrocatalytic performance of Mn_3O_4/CMK-3 composite is due to its unique structure. In recent years, the "three-phase interface electrocatalytic reaction" of gas has been one of the focuses of present science studies. Thereby, it can be assumed that this simple synthesis method and the advance structure can be applied in other field (e.g., electrocatalytic reaction of CO_2, H_2, or CO, etc.).

Acknowledgment. This work was partially supported by the National Natural Science Foundation of China (No. 20633040).

CM062685T